

PAPER

CrossMark
click for updatesCite this: *CrystEngComm*, 2015, 17, 2642

Controlled synthesis of mesocrystal magnesium oxide parallelogram and its catalytic performance

Xiaoling Zhang,^a Yajun Zheng,^a Haijun Yang,^b Qian Wang^a and Zhiping Zhang^{*a}

Mesocrystal magnesium oxide (MgO) parallelogram with lengths of diagonal line in the range of 7–9 μm has been synthesized through a facile precipitation method by using phosphate species as the morphology regulator and $\text{Mg}(\text{NO}_3)_2$ and $\text{Na}_2\text{C}_2\text{O}_4$ as the inorganic sources. Scanning electronic microscope examination revealed that there is a canyon in the middle of the diagonal line of the as-synthesized products. The canyon resulted from the self-assembly of layer-like structures with a thickness of around 100–150 nm on both sides. To investigate the effect of reaction conditions on the morphologies and components of the resulting products, the types and addition amount of phosphate species and the reaction temperature were studied in detail. The results demonstrated that the introduction of trace amounts of phosphate species in the reaction system played a crucial role in determining the morphologies of the obtained products with variation of reaction temperatures, whereas their components have little been influenced after analyses by Fourier-transform infrared spectroscopy and X-ray diffraction. When as-synthesized mesocrystal MgO was employed as a catalyst in the Meerwein–Ponndorf–Verley (MPV) reaction between benzaldehyde and ethanol, it demonstrated superior performance to MgO particles without the presence of phosphate species.

Received 21st January 2015,
Accepted 12th February 2015

DOI: 10.1039/c5ce00136f

www.rsc.org/crystengcomm

1. Introduction

Controlled synthesis of inorganic materials with desirable morphologies plays an important role in the development of new materials due to the strong relationship between physical properties and morphologies.^{1,2} Magnesium oxide, a typical wide band gap insulator with a band gap of 7.8 eV, has been extensively used as a magnetic tunnel junction for semiconductor spintronics, as an additive in refractory experiments due to its high thermal stability, and as a component of high temperature superconductor products and catalysts.^{3–5} MgO has also demonstrated its promise in the adsorption of many pollutants.^{6,7} In recent years, numerous studies have demonstrated that the performance of MgO is highly influenced by its morphologies.^{5,8–11} For example, many reports have evidenced that the catalytic performance of MgO was closely related to its shape, illustrating an apparent morphology-dependent phenomenon.⁹ Sutradhar *et al.* observed that the extent of the catalytic properties of MgO was highly controlled by its morphology.⁸ Namely, the shapes of flowers and house-of-cards were highly active for the condensation reaction of benzaldehyde with acetophenone owing to the presence of

large amounts of step edges and corners, low coordinated sites and lattice defects. MgO nanoflakes demonstrated high reactivity in the condensation reaction between benzaldehyde and acetophenone resulting from their high surface area. Wang *et al.* reported that MgO nanosheets and nanodisks showed much higher reaction rates than nanofibers because of their large numbers of surface basic sites.⁹ Therefore, the catalytic, adsorption, electronic, optical, and magnetic properties of MgO can be tailored by controlling its morphology.

Up to now, various methods, including template synthesis,¹² hydrothermal method,¹¹ chemical vapor deposition,¹³ precipitation method,^{14,15} precursor decomposition,¹⁶ sol–gel technique¹⁷ and so on,^{18,19} have been developed for the preparation of different morphologies of MgO. The reported morphologies of MgO are mainly composed of spherical structures,¹⁴ nanowires, nanotubes or nanobelts,²⁰ nanoflowers,²¹ nanosheets,²² cubes,²³ whiskers,²⁴ stacks of plates,²⁵ rectangular parallelepiped structures,²⁶ columnar structures²⁷ and coralline.²⁸ In this study, MgO with a unique morphology of parallelogram has been synthesized *via* facile precipitation. In the previous investigation,¹⁴ we found that the morphology of spherical MgO could be well tailored by using trace amounts of phosphate species as the morphology regulator and commercial $\text{Mg}_5(\text{CO}_3)_4(\text{OH})_2 \cdot 4\text{H}_2\text{O}$ solution as the seed in the reaction system of $\text{Mg}(\text{NO}_3)_2$ and K_2CO_3 . Using this method, a suture in the middle of the spherical-like MgO precursor, $\text{Mg}_5(\text{CO}_3)_4(\text{OH})_2 \cdot 4\text{H}_2\text{O}$, can be elaborately smoothed

^a School of Chemistry and Chemical Engineering, Xi'an Shiyou University, Xi'an 710065, China. E-mail: zhangzp0304@gmail.com; Fax: +86 29 8838 2693; Tel: +86 29 8838 2694

^b Department of Chemistry, Tsinghua University, Beijing 100084, China

by addition of phosphate species, and the formation rate of spherical $\text{Mg}_5(\text{CO}_3)_4(\text{OH})_2 \cdot 4\text{H}_2\text{O}$ can be accelerated by addition of trace amounts of $\text{Mg}_5(\text{CO}_3)_4(\text{OH})_2 \cdot 4\text{H}_2\text{O}$ seeds. However, the effect of phosphate species on the morphologies and properties of the resulting products in other reaction systems is still unclear. To gain further insight into the capacities of phosphate species, this study systematically investigated the evolution of the MgO precursor magnesium oxalate with the addition of phosphate species in the reaction between $\text{Mg}(\text{NO}_3)_2$ and $\text{Na}_2\text{C}_2\text{O}_4$. The influence of the types of phosphate species (*e.g.*, sodium phosphate, sodium tripolyphosphate and sodium polyphosphate), the addition amount of sodium tripolyphosphate and the reaction temperature on the morphologies of the obtained products have been examined in detail. Also, a comparison has been made between the catalytic performance of the obtained products without and in the presence of sodium tripolyphosphate for the MPV reaction of benzaldehyde and ethanol.

2. Experimental

2.1 Synthesis of MgO parallelogram

In a typical procedure, 10.26 g of $\text{Mg}(\text{NO}_3)_2 \cdot 6\text{H}_2\text{O}$ was dissolved into 25 mL of double-deionized water, and the solution pH value was 6.6. Then, the $\text{Mg}(\text{NO}_3)_2$ solution was transferred into a 250 mL three-necked flask and heated to 323 K. Subsequently, 0.05 g of sodium tripolyphosphate was added into 125 mL of 0.4 M $\text{Na}_2\text{C}_2\text{O}_4$ solution, and the mixture was also heated to 323 K. Under vigorous stirring (*ca.* 800 rpm), the $\text{Na}_2\text{C}_2\text{O}_4$ mixture solution with a pH value of 7.1 was poured into the $\text{Mg}(\text{NO}_3)_2$ solution in 4–5 s. The mixture was further stirred for 1 min and then maintained at a temperature of 323 K under static conditions for 1 h. After that, a white precipitate was collected, filtered off, and washed with double-deionized water and ethanol several times. The MgO sample was prepared by calcination of the $\text{MgC}_2\text{O}_4 \cdot 2\text{H}_2\text{O}$ parallelogram in air from room temperature to 573 K with a rate of 2 K min^{-1} for 2 h. After that, the product was calcined from room temperature to 823 K in a muffle furnace and then maintained at that temperature for 6 h.

2.2 Characterization

The crystal structures of the as-synthesized products were characterized by X-ray diffraction (XRD) on a XRD-6000 diffractometer using $\text{Cu K}\alpha$ radiation. The operation voltage was 40 kV, and the current was 30 mA. The morphology and size of the obtained particles were examined by a JEOL JSM-6390A scanning electron microscope (SEM) and a FEI Tecnai G2 F20 transmission electron microscope (TEM). The IR spectra of the obtained samples were recorded with a Bruker vertex 70 series FT-IR spectrometer in transmission mode in the range of $4000\text{--}400 \text{ cm}^{-1}$. The resolution was 4 cm^{-1} and eight scans were signal-averaged in each interferogram. Nitrogen adsorption–desorption isotherms were obtained using a Micrometrics ASAP 2020HD88 instrument at 77 K.

2.3 Catalytic evaluation

The catalysts were evaluated by using the MPV reaction between ethanol and benzaldehyde. In a typical reaction, ethanol (7.0 mL, 120 mmol), benzaldehyde (0.60 mL, 6 mmol), and as-synthesized MgO (1.0 g) were transferred into a 50 mL round-bottom flask fitted with a reflux condenser. The reaction mixture was heated to the reflux temperature (351 K) under magnetic stirring. The reaction solution was withdrawn in different intervals by using a micropipette during the reaction. The collected products were analyzed with an Agilent GC-7890B gas chromatograph equipped with a HP-INNOWax capillary column (30 m \times 0.32 mm I.D., 0.25 μm film thickness).

3. Results and discussion

SEM and TEM observation and powder XRD

The uniform mesocrystal MgO parallelogram was synthesized by using phosphate species (sodium tripolyphosphate or sodium polyphosphate) as the morphology regulator of $\text{MgC}_2\text{O}_4 \cdot 2\text{H}_2\text{O}$, and $\text{Mg}(\text{NO}_3)_2$ and $\text{Na}_2\text{C}_2\text{O}_4$ as the inorganic sources. The reaction mixture was stirred vigorously for 1 min and then maintained under static conditions for reaction. Fig. 1 shows the typical SEM and TEM images and XRD pattern of parallelogrammic MgO obtained by calcination of their precursors, which were prepared by directly pouring $\text{Na}_2\text{C}_2\text{O}_4$ into $\text{Mg}(\text{NO}_3)_2$ solution in the presence of 0.05 g of sodium tripolyphosphate. Fig. 1a demonstrates the lower-magnification SEM image of the as-synthesized monodisperse parallelogram. It is obvious that the particles are parallelogrammic products with lengths of diagonal line in the range of 7–9 μm , and the average length is about 8.6 μm . Fig. 1b presents the magnified view of an individual parallelogram. It has been found by careful observation that there is a canyon in the middle of the diagonal line of the as-synthesized product. The canyon resulted from the self-assembly of layer-like structures with a thickness of *ca.* 100–150 nm on both sides, and the detailed structures of the canyon and the layer-like structures on both sides of the canyon are shown in Fig. 1c and d. However, on both ends of the diagonal line of the as-synthesized product, it is interesting that the corresponding regions become relatively flat (Fig. 1b). Fig. 1e shows the TEM image of an individual parallelogram, further illustrating the detailed structure of the synthesized parallelogram particle. Although the MgO parallelogram demonstrates a uniform structure (Fig. 1b–e), the 3D hierarchical structure illustrates that it is structurally polycrystalline in nature (Fig. 1f) and is made of domains of single crystalline nanoparticles and amorphous particles as indicated by the HRTEM images (Fig. 1g–i), and increasing the reaction temperature and aging time favors the growth of crystalline nanoparticles as shown in Fig. 1i. The HRTEM dark-field image (Fig. 1j) clearly demonstrates that the single crystalline nanoparticles are distributed in the as-prepared MgO bulk particles. These results revealed that the as-prepared MgO micrometer-sized particles have the characteristic of

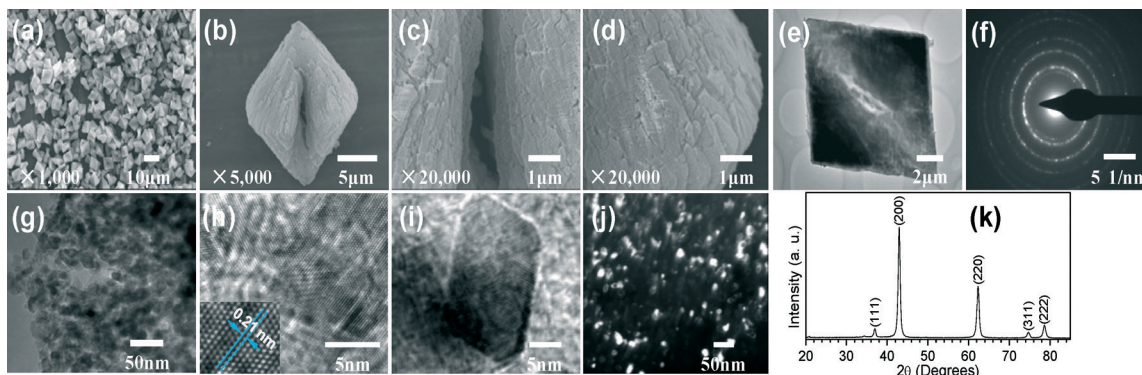


Fig. 1 Typical SEM images of parallelogrammic MgO synthesized by the calcination of its precursor which was obtained by pouring $\text{Na}_2\text{C}_2\text{O}_4$ into $\text{Mg}(\text{NO}_3)_2$ solution in the presence of 0.05 g of sodium triphosphosphate at 323 K followed by a period of 1 h aging: (a) panoramic morphologies, (b) individual parallelogram, (c) and (d) detailed view of the surface structure of an individual particle, (e) typical TEM image of parallelogrammic MgO, (f) selected area electron diffraction pattern of MgO, (g) HRTEM image showing the fine structure of the MgO parallelogram, (h) and (i) HRTEM image of single crystalline domains of MgO, (j) HRTEM dark-field image and (k) XRD pattern of as-synthesized MgO. Note: (1) the MgO particles for (i) were prepared by pouring $\text{Na}_2\text{C}_2\text{O}_4$ into $\text{Mg}(\text{NO}_3)_2$ solution in the presence of 0.05 g of sodium triphosphosphate at 323 K followed by 1 h aging, and then the aging temperature was increased up to 373 K; (2) the inset in (h) is the enlarged crystallite surface used for measuring the d spacing between two consecutive lattice planes.

mesocrystal materials.^{29–31} Although up to now different mesocrystal materials, including biomimetic materials,^{32,33} metal oxides,^{34–37} metal particles^{38–41} and other inorganic materials,^{42–44} have been extensively studied, little investigation on MgO mesocrystals has been reported.⁴⁵ This study presents one example of the preparation of an MgO mesocrystal. The detailed surface structure illustrates that the crystallite size varies in the range of 0.5–5 nm (Fig. 1g), and the d spacing between two consecutive lattice planes is 0.21 nm (Fig. 1h), suggesting the preferential growth of thermodynamically stable (200) planes. The crystal structures of the as-synthesized products were further confirmed by XRD. As shown in Fig. 1k, all diffraction peaks in the XRD pattern can be readily indexed to the cubic phase of MgO with a lattice constant of $a = 4.213$, in good agreement with the values reported in the literature (JCPDS card: 4-829). Also, no other impurities were detected by XRD (Fig. 1k), indicating that the presence of trace amounts of sodium triphosphosphate almost has no effects on the phase of the final product.

Influence of phosphate species

To better understand the formation of parallelogrammic MgO, the influence of reaction conditions on the morphologies of MgO precursors was examined in detail. In the previous report of Zhang *et al.*,¹⁴ the addition of trace amounts of phosphate species had a great influence on the morphology of $\text{Mg}_5(\text{CO}_3)_4(\text{OH})_2 \cdot 4\text{H}_2\text{O}$ during the precipitation of magnesium nitrate and potassium carbonate. The added phosphate species can erase an obvious suture in the middle of spherical-like particles due to the strong complexing interaction between Mg^{2+} and phosphate ions absorbed on the surface of the crystals.^{14,46,47} The influence of phosphates on the morphologies of the products increased with the increase in the polymerization degree of phosphates.^{14,47} In the present study, the influence of various phosphate species (*e.g.*,

sodium phosphate and sodium polyphosphate) on the morphologies of the products was investigated. Fig. 2 shows the

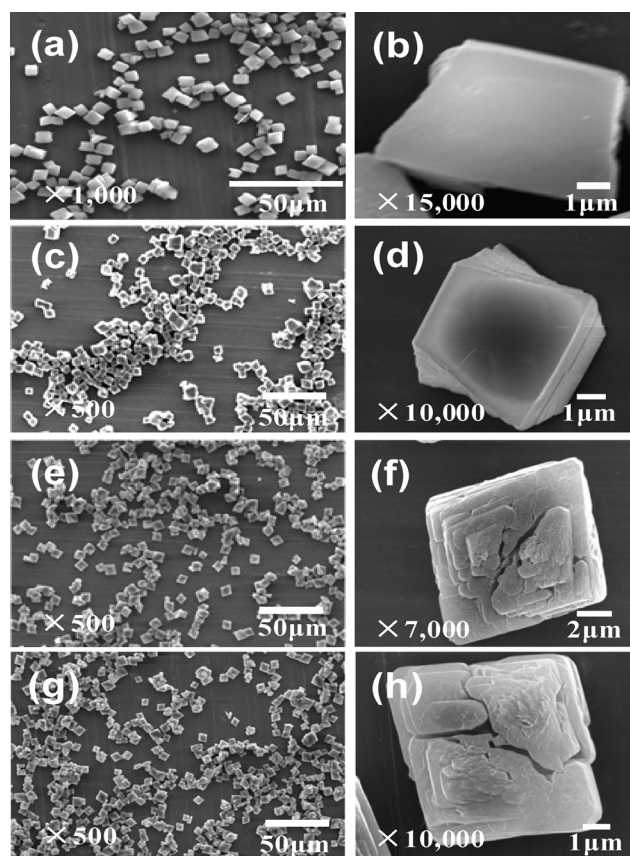


Fig. 2 SEM images of MgO precursors obtained by adding different types of phosphate species at 323 K: (a) and (b) without addition of any phosphate species; (c) and (d) 0.05 g of sodium phosphate; (e) and (f) 0.05 g of sodium triphosphosphate; and (g) and (h) 0.05 g of sodium polyphosphate. (b), (d) (f) and (h) are the corresponding representative particles in (a), (c), (e) and (g).

effect of phosphate species on the morphology of MgO precursors. Apparently, the addition of phosphate species has a pronounced effect on their morphologies. When there is no phosphate salt in the reaction system, the product is mainly composed of trapezoidal particles (Fig. 2a and b), similar to the recent investigation done by Zhu *et al.*⁴⁸ With the addition of 0.05 g of sodium phosphate, the morphology of the obtained product changed from a relatively regular trapezoid to a trapezoid-like structure containing different layers as shown in Fig. 2c and d. With the increase in the polymerization degree of phosphate salt from sodium phosphate to sodium tripolyphosphate, the product demonstrates a mono-disperse parallelogram composed of layer-like structures (Fig. 2e). As discussed above, there is a canyon in the middle of the diagonal line of the as-synthesized product (Fig. 2f). Similar results were obtained for the reaction system containing 0.05 g of sodium polyphosphate as shown in Fig. 2g and h. It is clear that the influence of phosphate species on the morphologies of the obtained products increased with the polymerization degree of phosphates, which is in good agreement with previous reports.^{14,47} However, different from the effect of phosphates on the morphology of $\text{Mg}_5(\text{CO}_3)_4(\text{OH})_2 \cdot 4\text{H}_2\text{O}$, addition of phosphates into the reaction system of $\text{MgC}_2\text{O}_4 \cdot 2\text{H}_2\text{O}$ makes the layer-like structures of the obtained product more obvious, even changing its basic morphology from a trapezoid to a parallelogram. These results suggest that with the variation of reaction systems, the complexing effect between Mg^{2+} and phosphates will change the shape of the final product into different morphologies.

In order to gain insight into the effect of different phosphate species on the morphologies of the resulting products, energy dispersive spectroscopy (EDS) analysis was carried out to determine the content of different phosphate species in a micrometer-sized particle. Fig. 3a and b show the typical micrometer-size particle used for EDS analysis and the corresponding analysis results. After analyzing the percentages of different atoms such as C, O, Mg and P in the selected particles, it can be seen from the list in Fig. 3c that the contents of C, O and Mg atoms were kept almost constant, whereas the percentage of P atom in the resulting particles gradually increased ranging from sodium phosphate to sodium tripolyphosphate, and then to sodium polyphosphate. These results indicate that the level of phosphate in the obtained particle is very low ($0.006 \pm 0.007\%$, namely, 0.0005 PO_4^{3-} molecule per MgC_2O_4 molecule), which is below the limit of detection of EDS analysis (0.1%). This case to a certain degree reveals the reason why the morphology of the obtained product in the presence of 0.05 g of sodium phosphate (Fig. 2c and d) is similar to that of the particles without the addition of any phosphate species (Fig. 2a and b). On the contrary, the content of tripolyphosphate in the particles from the reaction systems in the presence of 0.05 g of sodium tripolyphosphate and sodium polyphosphate is high enough, and the values are $0.192 \pm 0.032\%$ ($0.0047 \text{ P}_3\text{O}_{10}^{5-}$ molecule per MgC_2O_4 molecule) and $0.260 \pm 0.032\%$ ($0.0070 \text{ P}_3\text{O}_{10}^{5-}$ molecule per MgC_2O_4 molecule), respectively. This information suggests

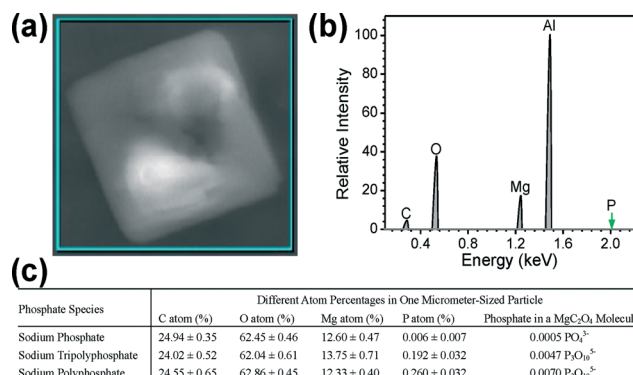


Fig. 3 (a) The typical SEM image of selected micrometer-sized particle used for EDS analysis, (b) the corresponding EDS analysis result, and (c) the different atom percentages (e.g., C, O, Mg and P atom) in one micrometer-sized particle with the variation of phosphate species (sodium phosphate, sodium tripolyphosphate and sodium polyphosphate) and the number of phosphate or tripolyphosphate molecules in a MgC_2O_4 molecule which is based on the different atom percentages in the selected particle. Note: (1) the different atom percentages are the average value from five different micrometer-size particles; (2) $\text{P}_3\text{O}_{10}^{5-}$ is used to calculate the number of phosphate species in a MgC_2O_4 molecule due to the unavailable formula structure of sodium polyphosphate; (3) the Al peak in Fig. 3(b) is from the background matrix.

that in the reaction systems of sodium tripolyphosphate and sodium polyphosphate, the phosphate species are prone to interact with the MgC_2O_4 molecule and participate in the formation of the MgC_2O_4 precipitate, thus leading to the disruption of the growth of MgC_2O_4 extended structures (Fig. 2e–f).

FT-IR spectroscopy is a useful tool to understand the functional groups of inorganic materials. This study investigated the spectra of the products from the reaction between $\text{Na}_2\text{C}_2\text{O}_4$ and $\text{Mg}(\text{NO}_3)_2$ in the presence of different types of phosphate species. With the variation in the polymerization degree of the phosphate species from sodium phosphate to sodium polyphosphate, the IR spectra (data not shown) were kept constant and had the characteristic adsorption bands of $\text{MgC}_2\text{O}_4 \cdot 2\text{H}_2\text{O}$.^{16,49} These results suggest that the addition of trace amounts of phosphate species has almost no effects on the IR adsorption bands of the obtained products.

For the purpose of investigating the relationship between the crystallite structures of the obtained products and the phosphate species, the XRD patterns of MgO precursors obtained by adding different types of phosphate species at 323 K were examined (Fig. 4). It is obvious that the XRD patterns are very similar, and can be indexed to magnesium oxalate dihydrate ($\text{MgC}_2\text{O}_4 \cdot 2\text{H}_2\text{O}$, JCPDS card: 28-0625). No characteristic peaks of impurities such as phosphate salts or other by-products were observed, indicating that the addition of phosphate species has no influence on the components of the resulting products, which is consistent with the IR analysis above. However, by careful examination of these spectra, it can be found that the peak intensity (e.g., (200), ($\bar{4}$ 02) and ($\bar{6}$ 02)) gradually decreased with an increase in the

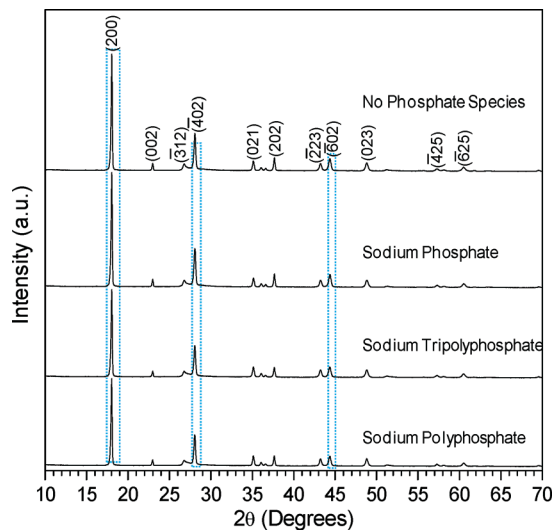


Fig. 4 Typical XRD patterns of MgO precursors obtained by adding different types of phosphate species at 323 K. (Note: no phosphate species means that the reaction system did not contain any phosphate species, and the product was obtained by pouring $\text{Na}_2\text{C}_2\text{O}_4$ into $\text{Mg}(\text{NO}_3)_2$ solution. Sodium phosphate, sodium tripolyphosphate and sodium polyphosphate, respectively, denotes the products obtained by pouring $\text{Na}_2\text{C}_2\text{O}_4$ into $\text{Mg}(\text{NO}_3)_2$ solution in the presence of 0.05 g sodium phosphate, sodium tripolyphosphate and sodium polyphosphate.)

polymerization degree of phosphate salts, especially sodium tripolyphosphate and sodium polyphosphate. As well known, phosphate can form the undissolved compound $\text{Mg}_3(\text{PO}_4)_2$ with Mg^{2+} due to the small solubility product constant ($K_{\text{sp}}(\text{Mg}_3(\text{PO}_4)_2) = 9.8 \times 10^{-25}$). So when the reaction system contains a little amount of sodium phosphate, PO_4^{3-} will interact with Mg^{2+} and more favorably produce a $\text{Mg}_3(\text{PO}_4)_2$ precipitate than Mg^{2+} with $\text{C}_2\text{O}_4^{2-}$ owing to its higher $K_{\text{sp}}(\text{MgC}_2\text{O}_4) = 8.6 \times 10^{-5}$. Accordingly, $\text{Mg}_3(\text{PO}_4)_2$ nuclei will first be produced, and with the exhaustion of PO_4^{3-} ions in the reaction system, $\text{C}_2\text{O}_4^{2-}$ will interact with Mg^{2+} to form a MgC_2O_4 precipitate followed by self-assembly into a trapezoid-like structure (Fig. 2c and d). As mentioned above (Fig. 3c),

a very little amount of P atom was determined in the micrometer-sized particles in the presence of 0.05 g of sodium phosphate, which further confirms that the $\text{Mg}_3(\text{PO}_4)_2$ precipitate does not participate in the nucleation and self-assembly of MgC_2O_4 particles. As a result, little effect was observed in the XRD pattern (Fig. 4b) of the obtained product. On the contrary, Mg^{2+} can form a stable soluble complex compound with sodium tripolyphosphate or polyphosphate. The resulting complex compound, on the one hand, would decrease the supersaturation degree of Mg^{2+} in aqueous solution, and prevent the growth of $\text{MgC}_2\text{O}_4 \cdot 2\text{H}_2\text{O}$.⁵⁰ More importantly, the polyphosphate ions with high charge density will interact with Mg^{2+} at the surface of the formed $\text{MgC}_2\text{O}_4 \cdot 2\text{H}_2\text{O}$, thus blocking the active growth sites of $\text{MgC}_2\text{O}_4 \cdot 2\text{H}_2\text{O}$.⁵¹ The higher content of P atom in the obtained particles (Fig. 3c) also suggests that tripolyphosphate or polyphosphate participates in the reaction between Mg^{2+} and $\text{C}_2\text{O}_4^{2-}$. Accordingly, the peak intensity in the XRD patterns became weaker in contrast to those of the products without phosphate species (Fig. 4). Owing to the blocking effect of polyphosphate salts, the self-assembly behavior of $\text{MgC}_2\text{O}_4 \cdot 2\text{H}_2\text{O}$ also exhibits a great change, and the final morphologies of the obtained products have much difference from the systems without the presence of polyphosphate salts as shown in Fig. 2.

Influence of the amount of tripolyphosphate

Fig. 5 shows the typical SEM images of the MgO precursors obtained by pouring $\text{Na}_2\text{C}_2\text{O}_4$ into $\text{Mg}(\text{NO}_3)_2$ solution in the presence of various amounts of sodium tripolyphosphate (STPP). When there is no STPP in the reaction system, the product demonstrates a trapezoid-like structure (Fig. 5a). With the addition of 0.05 g of STPP, it is interesting that monodisperse parallelogram particles composed of layer-like structures were obtained, and there is a canyon in the middle of the diagonal line of the as-synthesized product (Fig. 5b). Further increasing the amount of STPP from 0.1–0.15 g, the canyon in the particle gradually disappeared, and the surface of the product became relatively flat although it is still

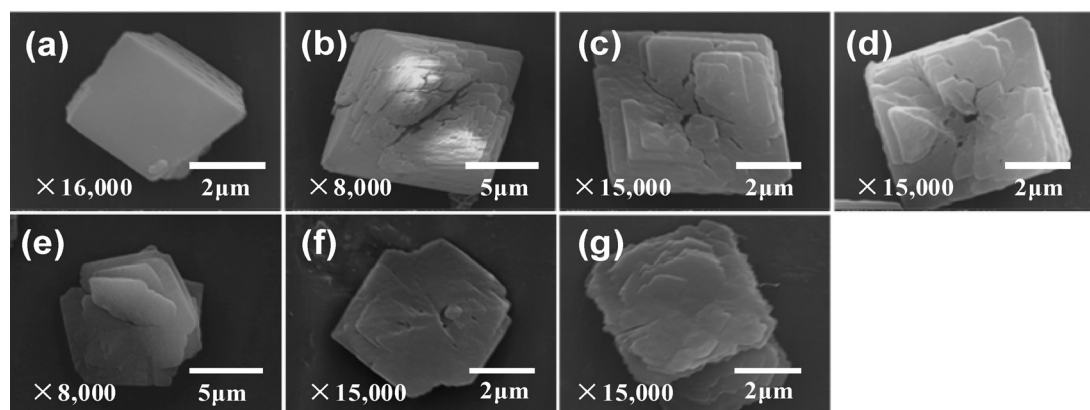


Fig. 5 Typical SEM images of MgO precursors obtained by pouring $\text{Na}_2\text{C}_2\text{O}_4$ into $\text{Mg}(\text{NO}_3)_2$ solution in the presence of various amounts of sodium tripolyphosphate: (a) 0 g; (b) 0.05 g; (c) 0.1 g; (d) 0.15 g; (e) 0.2 g; (f) 0.3 g; and (g) 0.5 g at 323 K.

composed of layer-like structures (Fig. 5c–d). When the amount of STPP was 0.2 g, the obtained product was self-assembled by obvious layer-like structures (Fig. 5e). With the increase in the amount of STPP to 0.3 g, the product turned into a square-like structure with the loss of two opposite corners (Fig. 5f). The obtained product demonstrates a regular layer-like square structure when the amount of STPP is 0.5 g as shown in Fig. 5g. These results suggest that in the reaction system of $\text{MgC}_2\text{O}_4 \cdot 2\text{H}_2\text{O}$, the morphologies of the products are highly dependent on the addition amount of STPP, which could vary the morphologies from a trapezoid-like structure to a parallelogram, then to a square-like structure. Besides that, the basic composition unit of the particles, namely, the layer-like structure, also demonstrates different self-assembly forms with the variation of the amount of STPP. Although the amount of STPP or other phosphate species has a great influence on the morphologies of the obtained products in the literature,^{14,52} the basic form of the particles was kept almost constant. In the present study, it can be observed that the morphologies of the resulting products significantly varied with the addition of STPP, illustrating that phosphate species play a more significant role in determining the final morphologies of $\text{MgC}_2\text{O}_4 \cdot 2\text{H}_2\text{O}$ than those of spherical $\text{Mg}_5(\text{CO}_3)_4(\text{OH})_2 \cdot 4\text{H}_2\text{O}$ ¹⁴ or spindle-type hematite particles.⁵²

Although STPP has a great effect on the morphologies of the final products, the chemical composition of the final precipitate formed in the reaction solution was kept almost constant (Fig. 6), which is consistent with previous reports.^{14,52} Fig. 6a shows the XRD patterns of the obtained products from the systems in the presence of different amounts of STPP. As can be seen, all the XRD patterns can be indexed to $\text{MgC}_2\text{O}_4 \cdot 2\text{H}_2\text{O}$ (JCPDS card: 28-0625). By careful observation, it can be found that with the increase in the addition amount of STPP in the reaction system of $\text{Na}_2\text{C}_2\text{O}_4$ and $\text{Mg}(\text{NO}_3)_2$, all the diffraction peak intensities such as (200) and $(\bar{6}25)$ gradually decrease. Even more, some diffraction peaks (e.g., $(\bar{3}12)$ and $(\bar{4}25)$) became much weaker. As discussed above, the

influence of STPP on the crystal structures of the final products is *via* the interaction between STPP and Mg^{2+} at the surface of the formed $\text{MgC}_2\text{O}_4 \cdot 2\text{H}_2\text{O}$, which blocks the active growth sites of $\text{MgC}_2\text{O}_4 \cdot 2\text{H}_2\text{O}$.⁵¹ Due to the blocking effect, the growth speed of $\text{MgC}_2\text{O}_4 \cdot 2\text{H}_2\text{O}$ became slower and slower with the increase in the addition amount of STPP. Therefore, the crystal structure gradually became poor, which is directly reflected in the intensity of the diffraction peaks shown in Fig. 6a. Also, we examined the calcined products from the reaction system in the presence of different amounts of STPP, as shown in Fig. 6b. Similar to the XRD patterns in Fig. 6a, the intensity of all the diffraction peaks gradually decreased, revealing that the crystallization degree became poorer relative to the reaction system without STPP. These results demonstrate that the presence of STPP in the reaction system of $\text{Na}_2\text{C}_2\text{O}_4$ and $\text{Mg}(\text{NO}_3)_2$ can not only greatly vary the morphologies of the obtained products, but can also tailor the crystallization degree of the resulting products.

Influence of reaction temperature

In the previous study, it was found that the morphologies of $\text{MgCO}_3 \cdot x\text{H}_2\text{O}$ significantly varied with the reaction temperature.^{15,53} To investigate the effect of reaction temperature on the morphologies of $\text{MgC}_2\text{O}_4 \cdot 2\text{H}_2\text{O}$, we systematically examined the variation in the morphologies of the obtained products from 303–363 K with an increase in the addition amount of STPP. Fig. 7(a-1)–(g-1), (a-2)–(g-2) and (a-3)–(g-3) show the variation of the products with the amount of STPP at temperatures of 303 K, 343 K and 363 K. Similar to the products at 323 K, as shown in Fig. 5, the morphologies of the particles in products formed at 303 K and 343 K also varied from trapezoid-like structures to parallelogram, then to square-like structures. The difference between them is the variation of the surface structure of the products. For example, for the products with the addition of 0.1 g of STPP in the reaction system, the morphologies changed from parallelogram-like to

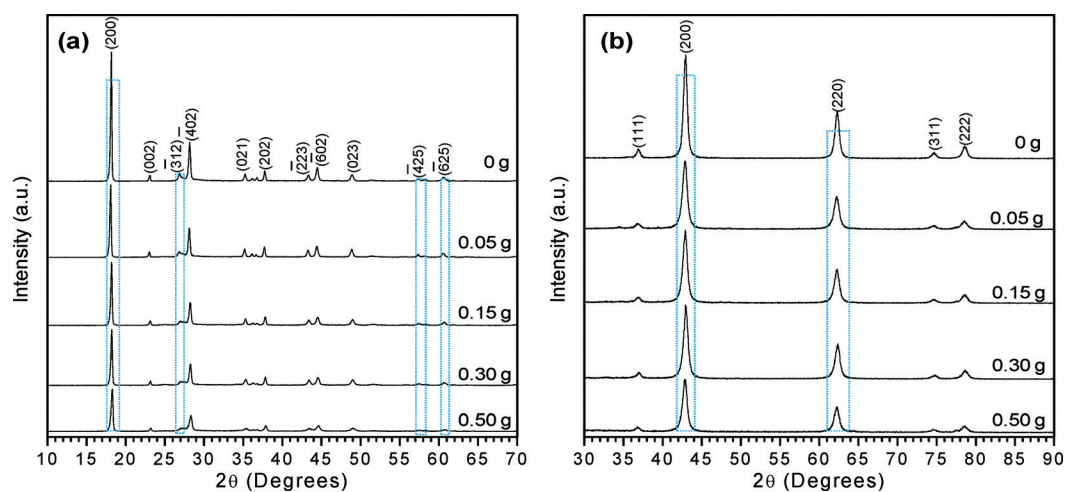


Fig. 6 Typical XRD patterns of (a) MgO precursors obtained by pouring $\text{Na}_2\text{C}_2\text{O}_4$ into $\text{Mg}(\text{NO}_3)_2$ solution in the presence of various amounts of sodium tripolyphosphate (0–0.5 g) at 323 K and (b) their corresponding calcined MgO products.

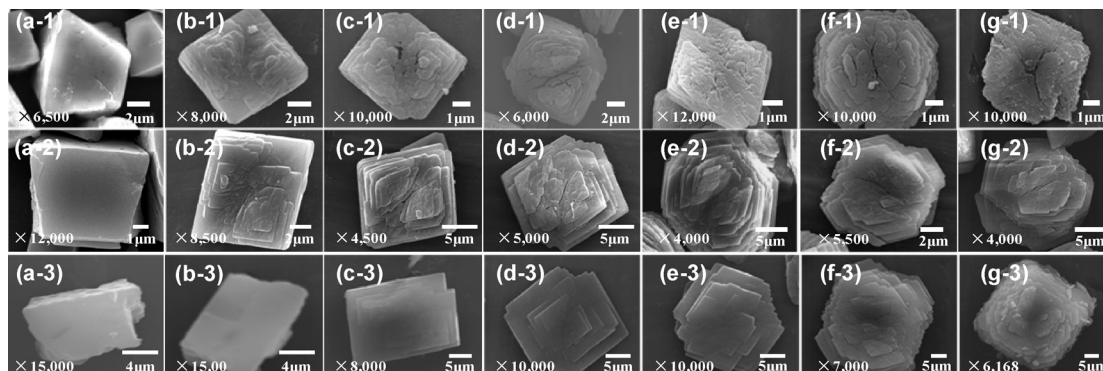


Fig. 7 Typical SEM images of MgO precursors obtained by pouring $\text{Na}_2\text{C}_2\text{O}_4$ into $\text{Mg}(\text{NO}_3)_2$ solution in the presence of various amounts of sodium tripolyphosphate at different reaction temperatures: (a) 0 g; (b) 0.05 g; (c) 0.1 g; (d) 0.15 g; (e) 0.2 g; (f) 0.3 g; and (g) 0.5 g at 303 K; (a-1)–(g-1) at 303 K, (a-2)–(g-2) at 343 K, and (a-3)–(g-3) at 363 K.

rectangle-like structures (Fig. 7(c-1), (c-2), (c-3) and 5c). The parallelogram-like products at a lower reaction temperature (e.g., 303 K) demonstrate a relatively flat surface structure. With the increase of reaction temperature, a canyon in the middle of the diagonal line of the as-synthesized product was self-assembled by some layer-like particles beside it. More interestingly, the canyon gradually becomes obvious as shown in Fig. 5c and 7(c-2). When 0.2 g of STPP was added into the reaction system, the morphologies of the resulting products changed from parallelogram-like structures assembled by unobvious layer-like units (Fig. 7(e-1)) to particles with obvious layer-like structures (Fig. 5e), then to products with petaloid-like structures (Fig. 7(e-2)), and finally to square-like structures with the loss of two opposite corners (Fig. 7(e-3)). From the discussion above, it is obvious that for the reaction system without STPP, the products demonstrate a relatively smooth surface structure (Fig. 5a and 7(a-1)–(a-3)). With the addition of STPP into the reaction solution, the obtained particles tend to become layer-like structures. From these results, it can be seen that the reaction temperature and the amount of STPP in the reaction system have significant effects on the self-assembly of the layer-like units, and finally change their morphologies.

Study of catalytic performance

To gain insight into the catalytic performance of the parallelogram-like MgO mesocrystal in the presence of STPP (Fig. 2e and f) and the trapezoid-like MgO without any STPP (Fig. 2a and b), the MPV reaction between benzaldehyde and ethanol was carried out. During the reaction, ethanol is oxidized to acetaldehyde, and benzaldehyde is reduced to benzyl alcohol. Fig. 8a compares the benzaldehyde conversion efficiency between both MgO materials at 351 K. It is obvious that the conversion efficiency of benzaldehyde gradually increased over the reaction time. Although the conversion of both MgO materials in the period of 0–8 h was close, much difference occurred after a reaction time of 8 h. For the trapezoid-like MgO particles, the value was kept almost constant with a conversion efficiency of around 58%, whereas

the reaction still proceeded for the parallelogram-like MgO mesocrystal. When the reaction time was 24 h, the conversion efficiency of benzaldehyde reached as high as 87%. These results demonstrate that the performance of the parallelogram-like MgO was superior to that of the trapezoid-like particles, probably attributable to the higher specific surface area ($69.3 \text{ m}^2 \text{ g}^{-1}$) or the unique surface structure, as mentioned above, of the former compared to that of the latter ($59.3 \text{ m}^2 \text{ g}^{-1}$).

In the MPV reaction, another side reaction occurred, which is accompanied by the conversion of benzaldehyde

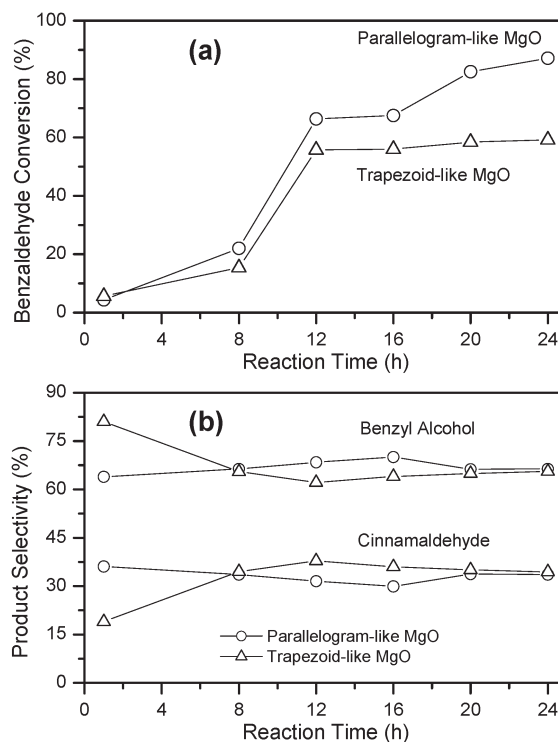


Fig. 8 Comparison of (a) benzaldehyde conversion and (b) product selectivity in the MPV reaction between benzaldehyde and ethanol at 351 K by using parallelogram-like MgO mesocrystal and trapezoid-like MgO as catalysts.

into benzyl alcohol. Namely, the resulting acetaldehyde from ethanol will further react with benzaldehyde to produce cinnamaldehyde.⁹ Fig. 8b compares the reaction selectivity for benzyl alcohol and cinnamaldehyde. Apparently, the selectivity for both products of the parallelogram-like MgO was kept almost constant with values of 67% and 33%, respectively, in the reaction period. But the trapezoid-like MgO demonstrated a higher selectivity in the first 8 h followed by a similar value to that of the parallelogram-like one. The reaction selectivity between both materials illustrates that the as-synthesized parallelogram-like MgO mesocrystal had more uniform surface properties than the trapezoid-like one in the MPV reaction.

Conclusions

In summary, mesocrystal MgO particles with a unique morphology of parallelogram were successfully synthesized by calcination of magnesium oxalate dihydrate which was prepared by the reaction of $\text{Mg}(\text{NO}_3)_2$ and $\text{Na}_2\text{C}_2\text{O}_4$ solution in the presence of trace amounts of phosphate species. To better understand the formation of the parallelogram-like particles, various experimental conditions were examined in detail. It was found that the type and addition amount of phosphate species as well as the reaction temperature played important roles in determining the final morphologies of magnesium oxalate dihydrate. For the reaction system without phosphate species, the products tend to become a smooth-surfaced structure. With the addition of phosphate species, the resulting particles turn into layer-like structures. The layer-like structure gradually becomes more obvious with the increase in the polymerization degree of phosphate species. Additionally, the self-assembly of the layer-like structures varies significantly with an increase in the reaction temperature. To gain insight into the performance of the parallelogram-like MgO mesocrystal, the MPV catalytic reaction between benzaldehyde and ethanol was carried out. The results demonstrated that the parallelogram-like mesocrystal had superior catalytic performance and surface properties to trapezoid-like MgO. We believe that this knowledge not only gives us an insight into the formation of parallelogram-like particles in the presence of polyphosphate salts, but also provides a facile way for the controlled synthesis of different morphologies of particles such as the parallelogram-like MgO mesocrystal, which may find widespread applications in catalysis and other fields. It should be pointed out here that the formation mechanism of the mesocrystal MgO parallelogram is also crucial to understand the self-assembly of the 3D structure. The corresponding investigation is still under way and will be reported in due course.

Acknowledgements

This work was supported by the National Natural Science Foundation of China (no. 21205093), the Education Department of Shaanxi Province (no. 2013JK0674), the Key Science

and Technology Program of Shaanxi Province of China (no. 2014K13-16), and the Xi'an Science and Technology Project in China (no. CXY1434(6)).

References

- 1 J. Xiang, W. Lu, Y. Hu, Y. Wu, H. Yan and C. M. Lieber, *Nature*, 2006, **441**, 489–493.
- 2 F. Patolsky, B. P. Timko, G. Yu, Y. Fang, A. B. Greytak, G. Zheng and C. M. Lieber, *Science*, 2006, **313**, 1100–1104.
- 3 B. Eckhardt, E. Ortel, J. Polte, D. Bernsmeier, O. Gorke, P. Strasser and R. Kraehnert, *Adv. Mater.*, 2012, **24**, 3115–3119.
- 4 Y. Lv, Z. Zhang, Y. Lai, J. Li and Y. Liu, *CrystEngComm*, 2011, **13**, 3848.
- 5 K. Zhu, J. Hu, C. Kübel and R. Richards, *Angew. Chem.*, 2006, **118**, 7435–7439.
- 6 Z. Zhang, Y. Zheng, J. Zhang, J. Chen and X. Liang, *J. Chromatogr. A*, 2007, **1165**, 116–121.
- 7 J. Jin, Y. Li, Z. Zhang, F. Su, P. Qi, X. Lu and J. Chen, *J. Chromatogr. A*, 2011, **1218**, 9149–9154.
- 8 N. Sutradhar, A. Sinhamahapatra, S. K. Pahari, P. Pal, H. C. Bajaj, I. Mukhopadhyay and A. B. Panda, *J. Phys. Chem. C*, 2011, **115**, 12308–12316.
- 9 F. Wang, N. Ta and W. Shen, *Appl. Catal., A*, 2014, **475**, 76–81.
- 10 J. V. Stark and K. J. Klabunde, *Chem. Mater.*, 1996, **8**, 1913–1918.
- 11 K. J. Klabunde, J. Stark, O. Koper, C. Mohs, D. G. Park, S. Decker, Y. Jiang, I. Lagadic and D. Zhang, *J. Phys. Chem.*, 1996, **100**, 12142–12153.
- 12 W.-C. Li, A.-H. Lu, C. Weidenthaler and F. Schuth, *Chem. Mater.*, 2004, **16**, 5676–5681.
- 13 E. Knözinger, O. Diwald and M. Sterrer, *J. Mol. Catal. A: Chem.*, 2000, **162**, 83–95.
- 14 Z. Zhang, Y. Zheng, J. Chen, Q. Zhang, Y. Ni and X. Liang, *Adv. Funct. Mater.*, 2007, **17**, 2447–2454.
- 15 Z. Zhang, Y. Zheng, J. Zhang, Q. Zhang, J. Chen, Z. Liu and X. Liang, *Cryst. Growth Des.*, 2007, **7**, 337–342.
- 16 F. Mohandes, F. Davar and M. Salavati-Niasari, *J. Phys. Chem. Solids*, 2010, **71**, 1623–1628.
- 17 H. Minami, K. Kinoshita, T. Tsuji and H. Yanagimoto, *J. Phys. Chem. C*, 2012, **116**, 14568–14574.
- 18 P. Tian, X.-Y. Han, G.-L. Ning, H.-X. Fang, J.-W. Ye, W.-T. Gong and Y. Lin, *ACS Appl. Mater. Interfaces*, 2013, **5**, 12411–12418.
- 19 L. De Matteis, L. Custardoy, R. Fernández-Pacheco, C. Magén, J. M. de la Fuente, C. Marquina and M. R. Ibarra, *Chem. Mater.*, 2012, **24**, 451–456.
- 20 Y. Yan, L. Zhou, J. Zhang, H. Zeng, Y. Zhang and L. Zhang, *J. Phys. Chem. C*, 2008, **112**, 10412–10417.
- 21 X. S. Fang, C. H. Ye, L. D. Zhang, J. X. Zhang, J. W. Zhao and P. Yan, *Small*, 2005, **1**, 422–428.
- 22 C. Yan, C. Sun, Y. Shi and D. Xue, *J. Cryst. Growth*, 2008, **310**, 1708–1712.
- 23 Z. Yimin, H. Yuexin and L. Guoliang, *Adv. Mater. Res.*, 2009, **92**, 35–40.
- 24 L. Xiang, F. Liu, J. Li and Y. Jin, *Mater. Chem. Phys.*, 2004, **87**, 424–429.

- 25 M. Sharma and P. Jeevanandam, *J. Alloys Compd.*, 2011, **509**, 7881–7885.
- 26 G. Wang, L. Zhang, H. Dai, J. Deng, C. Liu, H. He and C. T. Au, *Inorg. Chem.*, 2008, **47**, 4015–4022.
- 27 K.-H. Kim, M.-S. Lee, J.-S. Choi and J.-P. Ahn, *Thin Solid Films*, 2009, **517**, 3995–3998.
- 28 V. M. Boddu, D. S. Viswanath and S. W. Maloney, *J. Am. Ceram. Soc.*, 2008, **91**, 1718–1720.
- 29 H. Cölfen and M. Antonietti, *Angew. Chem., Int. Ed.*, 2005, **44**, 5576–5591.
- 30 R.-Q. Song and H. Cölfen, *Adv. Mater.*, 2010, **22**, 1301–1330.
- 31 L. Zhou and P. O'Brien, *J. Phys. Chem. Lett.*, 2012, **3**, 620–628.
- 32 Y.-Y. Kim, A. S. Schenk, J. Ihli, A. N. Kulak, N. B. J. Hetherington, C. C. Tang, W. W. Schmahl, E. Griesshaber, G. Hyett and F. C. Meldrum, *Nat. Commun.*, 2014, **5**.
- 33 C. You, Q. Zhang, Q. Jiao and Z. Fu, *Cryst. Growth Des.*, 2009, **9**, 4720–4724.
- 34 T. Li, Z. Cao, H. You, M. Xu, X. Song and J. Fang, *Chem. Phys. Lett.*, 2013, **555**, 154–158.
- 35 J. Fang, P. M. Leufke, R. Kruk, D. Wang, T. Scherer and H. Hahn, *Nano Today*, 2010, **5**, 175–182.
- 36 X. Liang, L. Gao, S. Yang and J. Sun, *Adv. Mater.*, 2009, **21**, 2068–2071.
- 37 S.-J. Liu, J.-Y. Gong, B. Hu and S.-H. Yu, *Cryst. Growth Des.*, 2008, **9**, 203–209.
- 38 J. Fang, B. Ding and X. Song, *Cryst. Growth Des.*, 2008, **8**, 3616–3622.
- 39 J. Fang, X. Ma, H. Cai, X. Song and B. Ding, *Nanotechnology*, 2006, **17**, 5841–5845.
- 40 J. Fang, B. Ding, X. Song and Y. Han, *Appl. Phys. Lett.*, 2008, **92**, 173120.
- 41 H. You, Y. Ji, L. Wang, S. Yang, Z. Yang, J. Fang, X. Song and B. Ding, *J. Mater. Chem.*, 2012, **22**, 1998.
- 42 J. Fang, B. Ding and H. Gleiter, *Chem. Soc. Rev.*, 2011, **40**, 5347–5360.
- 43 X. Fei, W. Li, Z. Shao, S. Seeger, D. Zhao and X. Chen, *J. Am. Chem. Soc.*, 2014, **136**, 15781–15786.
- 44 S. Chen and S. Yu, *Chin. Sci. Bull.*, 2009, **54**, 1854–1858.
- 45 T. Selvamani, T. Yagyu, S. Kawasaki and I. Mukhopadhyay, *Catal. Commun.*, 2010, **11**, 537–541.
- 46 A. Breeuwsma and J. Lyklema, *J. Colloid Interface Sci.*, 1973, **43**, 437–448.
- 47 C. Li and Y. Lü, *Int. J. Miner. Process.*, 1983, **10**, 219–235.
- 48 W. Zhu, L. Zhang, G.-L. Tian, R. Wang, H. Zhang, X. Piao and Q. Zhang, *CrystEngComm*, 2014, **16**, 308–318.
- 49 A. Kumar and J. Kumar, *J. Phys. Chem. Solids*, 2008, **69**, 2764–2772.
- 50 S. T. Liu, A. Hurwitz and G. H. Nancollas, *J. Urol.*, 1982, **127**, 351–355.
- 51 M. X. Zhao, H. Y. Yu, X. M. Wu and J. M. Ouyang, *Chinese Journal of Jinan University*, 2006, **27**, 705–709.
- 52 M. Ozaki, S. Kratochvil and E. Matijević, *J. Colloid Interface Sci.*, 1984, **102**, 146–151.
- 53 Z. P. Zhang, Y. J. Zheng, Y. W. Ni, Z. M. Liu, J. P. Chen and X. M. Liang, *J. Phys. Chem. B*, 2006, **110**, 12969–12973.

Copyright of CrystEngComm is the property of Royal Society of Chemistry and its content may not be copied or emailed to multiple sites or posted to a listserv without the copyright holder's express written permission. However, users may print, download, or email articles for individual use.